Journal of Statistical Physics, Vol. 48, Nos. 3/4, 1987

Bond Percolation in Two and Three Dimensions: Numerical Evaluation of Time-Dependent Transport Properties

G. A. van Velzen[1] and M. H. Ernst[1,2]

Received April 28, 1987

For random walks on two- and three-dimensional cubic lattices, numerical results are obtained for the static, $D(\infty)$, and time-dependent diffusion coefficient $D(t)$, as well as for the velocity autocorrelation function (VACF). The results cover all times and include linear and quadratic terms in the density expansions. Within the context of kinetic theory this is the only model in two and three dimensions for which the time-dependent transport properties have been calculated explicitly, including the long-time tails.

KEY WORDS: Lorentz gas; random walk on disordered lattice; ant in a labyrinth; bond percolation; random resistor network; lattice Green's functions.

1. INTRODUCTION

Random walks (RW) on disordered lattices are in many respects very similar to a Lorentz gas.[1] There exists a variety of problems that can be modeled by random walks on disordered lattices, such as dynamic percolation, ants-in-a-labyrinth and termite models, random resistor networks, and networks with normal and superelastic springs. Such problems have received much attention recently. The short-time behavior of the RW models is essentially described by an Enskog-type theory; at intermediate time scales the models show a strong "cage effect," in the sense that the velocity autocorrelation function (VACF) is negative for all positive times; at long times the RW models exhibit long-time tails, namely

[1] Instituut voor Theoretische Fysica, RUU, 3508 TA Utrecht, The Netherlands.
[2] Institute for Theoretical Physics, University of Florida, Gainesville, Florida 32611.

0022-4715/87/0800-0677$05.00/0 © 1987 Plenum Publishing Corporation

VACF $\sim t^{-1-d/2}$, which are essentially described by "repeated ring collisions."[1]

Because of these similarities it is of great interest to study the RW models on random lattices. The kinetic theory for the deterministic Lorentz gas becomes extremely complicated if one attempts to go beyond the contributions linear in the concentration c of scatterers or into intermediate-time regimes. Even the long-time tails for the 2D and 3D Lorentz gases have never been calculated to $O(c^2)$. Fortunately, the calculations for the RW models are considerably simpler, and through a combination of analytic and numerical methods we have obtained the static and time-dependent diffusion coefficients and VACF in two and three dimensions for *all* times, exact to $O(c^2)$. As far as we know, this is the only kinetic theory model in dimensions higher than one for which exact calculations have been performed in these time and density regimes.

As already indicated, kinetic theory methods for obtaining density expansions[1] of static and frequency-dependent transport properties can be applied succesfully to lattice models with quenched disorder, at least for densities not too close to a percolation threshold. This is shown by the results for the diffusion coefficient and the velocity autocorrelation function (VACF) in 2D lattice models with site[2,3] or bond[4] disorder. In this paper we will consider 2D and 3D models with bond disorder.

For the case of diluted randomness, where only a small fraction c of bonds or sites have been replaced at random by impurities, a kinetic theory has been developed for describing diffusion phenomena on random lattices.[5] Some properties of these models have been studied by other methods, such as the effective medium approximation (EMA),[6–9] renormalization group methods,[10] and the single-impurity approximation,[11,12] which is exact to linear order in the impurity concentration. For bond models EMA is also exact to $O(c)$, but for site models it is not.

However, until now, quantitative results covering the whole time interval from short times via intermediate times to long times have only been available for the velocity autocorrelation function to linear order in the impurity concentration c for this and related hopping models.[2,4]

In this paper we present numerical results for the 2D square and 3D cubic lattice bond models for both the VACF and the time-dependent diffusion coefficient, now including terms proportional to c^2. We also give the static diffusion coefficient for three dimensions up to $O(c^2)$. For the square lattice it was already given in Ref. 5.

In Section 2 we quote the results obtained in Ref. 5, including the expressions for the computation of the various quantities. In Section 3 we discuss the method used to calculate the lattice Green's functions for arbitrary lattice site. Further, in Section 4 we present the calculations per-

formed for the static diffusion coefficient in three dimensions. In Section 5 two methods for performing the Laplace inversion are discussed. Section 6 contains some remarks concerning the calculation of the time-dependent diffusion coefficient. Finally, in Section 7 the results for the VACF and the time-dependent diffusion coefficient are presented and discussed.

2. DENSITY EXPANSIONS

Here we confine ourselves to an outline of the theory developed by Ernst and Van Velthoven,[5] containing the expressions used in that paper.

The basic quantity studied in Ref. 5 is the probability distribution $P_{\mathbf{n}}(t)$ for a displacement $\mathbf{n}$ in a time t in a hopping model on a d-dimensional cubic lattice with unit lattice distance. Here, $p_{\mathbf{n}}(t)$ is an average over the quenched disorder. The most important quantity to be derived from $p_{\mathbf{n}}(t)$ is the mean square displacement $\langle n_x^2 \rangle(t)$ and the related time-dependent diffusion coefficient

$$D(t) = \frac{1}{2}\frac{\partial}{\partial t}\langle n_x^2 \rangle(t) = \int_0^t d\tau\, \varphi(\tau) \tag{2.1}$$

where $D(\infty) = D$ is the static diffusion coefficient and $\varphi(t)$ is the velocity autocorrelation function (VACF)

$$\varphi(t) = \langle v_x(0)\, v_x(t) \rangle = \frac{1}{2}\frac{\partial^2}{\partial t^2}\langle n_x^2 \rangle(t) \tag{2.2}$$

The model considered is that of an unbiased random walker (blind ant) that makes nearest neighbor hops and is hindered by the presence of randomly distributed bond impurities (scatterers). The lattice is a d-dimensional cubic lattice with $N = L^d$ sites and periodic boundary conditions. The sites are labeled by the vectors $\mathbf{n} \equiv (n_x, n_y, \ldots, n_d)$ and the bonds by $(\mathbf{n}, \alpha)$, where α runs from 1 to d. A fraction c of bonds in the host lattice (having "conductivity" $\sigma_0 = 1$) is replaced by impurity bonds with "conductivity" σ, which ranges from 0 ("hard scatterers"; percolation problem) to infinity ("superconducting" bonds, termite problem[14]).

For this problem, the continuous-time random walk is described by the probability distribution $p_{\mathbf{n}}(t)$, which satisfies the master equation

$$\begin{aligned} \dot{p}_{\mathbf{n}} &= \sum_{\alpha} \left[W^{\alpha}_{\mathbf{n}} p_{\mathbf{n}+\mathbf{e}_\alpha} + W^{\alpha}_{\mathbf{n}-\mathbf{e}_\alpha} p_{\mathbf{n}-\mathbf{e}_\alpha} - (W^{\alpha}_{\mathbf{n}} + W^{\alpha}_{\mathbf{n}-\mathbf{e}_\alpha}) p_{\mathbf{n}} \right] \\ &\equiv -\sum_{\alpha} \hat{L}_{\mathbf{nm}} p_{\mathbf{m}} = -(\hat{L}p)_{\mathbf{n}} \end{aligned} \tag{2.3}$$

with $\alpha = x, y, \ldots, d$; $W_{\mathbf{n}}^{\alpha}$ is the random variable assigned to the bond $(\mathbf{n}, \alpha)$:

$$W_{\mathbf{n}}^{\alpha} = \frac{1}{2d}(1 - bc_{\mathbf{n}}^{\alpha}) \tag{2.4}$$

with $b \equiv 1 - \sigma$, and $c_{\mathbf{n}}^{\alpha} = 1$ with probability c and $c_{\mathbf{n}}^{\alpha} = 0$ with probability $1 - c$. The $\mathbf{e}_{\alpha}$ is the unit vector in the positive α direction, and $\hat{L}_{\mathbf{nm}}$ is the coordinate representation of the linear master operator L.

It is shown that the probability distribution $p_{\mathbf{n}}(t)$ obeys the symmetry relation $p_{\mathbf{n}}(t, c, \sigma) = p_{\mathbf{n}}(\sigma t, 1 - c, 1/\sigma)$, from which follows, using (2.1) and (2.2),

$$D(c, \sigma) = \sigma D(1 - c, 1/\sigma) \tag{2.5}$$

for the static diffusion coefficient, and

$$\varphi(t, c, \sigma) = \sigma^2 \varphi(\sigma t, 1 - c, 1/\sigma) \tag{2.6}$$

The quantity of interest is the generating function of the moments of displacement, whose Fourier–Laplace transform is given by

$$F(\mathbf{q}, z) = \frac{1}{N} \sum_{\mathbf{n},\mathbf{m}} \{\exp[i\mathbf{q}(\mathbf{n} - \mathbf{m})]\} \langle \hat{p}_z(\mathbf{n} \mid \mathbf{m}) \rangle \equiv \langle (z + L)^{-1} \rangle_{\mathbf{qq}} \tag{2.7}$$

Here $\mathbf{q}$ is a reciprocal lattice vector in the first Brillouin zone (1BZ). The propagator $\hat{p}_z(\mathbf{n} \mid \mathbf{m}) = [(z + \hat{L})^{-1}]_{\mathbf{nm}}$ is the Laplace transform of $p(\mathbf{n}t \mid \mathbf{m}0)$, the conditional probability distribution. Its average is the analogue of the Van Hove self-correlation function $G_s(\mathbf{r}, t)$ in the theory of fluids.

With the help of (2.4) and (2.3), L can be decomposed into a part referring to a uniform lattice and a perturbation describing the influence of the impurities. In this manner, a density expansion is obtained for the response function $F(\mathbf{q}, z)$. The propagator of the uniform lattice is given by

$$g(\mathbf{q}) = \frac{1}{z + \omega(\mathbf{q})} \tag{2.8}$$

where $\omega(\mathbf{q})$ is defined as

$$\omega(\mathbf{q}) = \frac{1}{d} \sum_{\alpha} (1 - \cos q_{\alpha}) \tag{2.9}$$

A convenient definition in the course of our calculations is

$$G_{\alpha\beta}(\mathbf{n}, z) \equiv \int_{\mathbf{q}} \exp(-i\mathbf{q}\mathbf{n}) \frac{[1 - \exp(-iq_{\alpha})][1 - \exp(iq_{\beta})]}{z + \omega(\mathbf{q})} \tag{2.10}$$

Note that $\int[\exp(-i\mathbf{q}n)]/(z+\omega)$ is the probability for a displacement $\mathbf{n}$ on a uniform lattice, where we used the short-hand notation

$$\int_{\mathbf{q}} \cdots \equiv N^{-1} \sum_{\mathbf{q}\in 1\mathrm{BZ}} \cdots \underset{N\to\infty}{\simeq} (2\pi)^{-d} \int_{-\pi}^{\pi} \cdots \int_{-\pi}^{\pi} d^{(d)}\mathbf{q} \cdots \tag{2.11}$$

Further, a T-matrix resummation is carried out to account for successive visits of the random walker to the same impurity bond. The single impurity T-matrix is then introduced as

$$T(z) = \frac{b}{2d} \sum_{l=0}^{\infty} \left[\frac{bG_{\alpha\alpha}(\mathbf{0}, z)}{2d}\right]^l = \frac{b}{2d} \frac{1}{1-bJ(z)} \tag{2.12}$$

with

$$J(z) \equiv \frac{1}{d} \int_{\mathbf{q}} \frac{\omega(\mathbf{q})}{z+\omega(\mathbf{q})} \tag{2.13}$$

The final quantity to be defined is

$$R_{\alpha\beta}(\mathbf{n}, z) = T(z)\, G_{\alpha\beta}(\mathbf{n}, z) \tag{2.14}$$

Using these ingredients, it is possible to write down the response function. Here we are only interested in the mean square displacement $\langle n_x^2 \rangle$, diffusion coefficient $D(t)$, and VACF $\varphi(t)$. It follows from (2.2) that the Laplace transform $\Phi(z)$ of the VACF is given by

$$\Phi(z) = \frac{1}{2} z^2 \langle n_x^2 \rangle(z) = -\frac{1}{2} z^2 \frac{\partial^2}{\partial q_x^2} F(\mathbf{q}, z)\bigg|_{\mathbf{q}=0} \tag{2.15}$$

The expression for $\Phi(z)$, containing terms upto second order in the impurity concentration, obtained by Ernst and Van Velthoven[5] is

$$\begin{aligned}\Phi(z) = \frac{1}{2d} - cT(z) - c^2 T(z) \Big\{ & -2dT(z)\, J(z) \\ & + 4d^2 T(z)^2 \left[I(z) - J(z)^2\right] + \sum_{\mathbf{n}\neq 0} \frac{R_{xx}^3(\mathbf{n}, z)}{1 - R_{xx}(\mathbf{n}, z)} \\ & + (d-1) \sum_{\mathbf{n}} \frac{R_{xy}^4(\mathbf{n}, z)}{1 - R_{xy}^2(\mathbf{n}, z)} \Big\} + O(c^3)\end{aligned} \tag{2.16}$$

with

$$I \equiv J + z\, dJ/dz = (1/d) \int \mathbf{q}\omega^2/(z+\omega)^2$$

The $O(c)$ term accounts for all possible visits of the random walker to a single impurity, the $O(c^2)$ terms for all those to two different impurities. The last summation includes the $n=0$ term; Eq. (4.2) of Ref. 5 contains a misprint at this point.

The dependence on the impurity hopping rate $\sigma = 1-b$ occurs only through T, (2.12). For the special case of blocked bonds (bond percolation), where $b=1$, the coefficient of the c^2 term in (2.16) can be simplified further. With the help of the relations $I = J + z\,dJ/dz$ and $2dT(1-J)=1$ we find for $b=1$

$$-2dTJ + 4d^2T^2(I-J^2) = 4zd^2T^2\,dJ/dz \tag{2.17}$$

This relation can also be used as a test on the numerical accuracy.

3. ANALYSIS OF THE LATTICE FUNCTIONS

In the sequel we study the behavior of R_{xx} and R_{xy} as functions of the Laplace variable z and the lattice vector $\mathbf{n}$. In fact, as we conclude from (2.14), we need to calculate the quantities $G_{\alpha\beta}(\mathbf{n}, z)$ for general z. As we observe from (2.10), we can write $G_{\alpha\beta}(\mathbf{n}, z)$, following Ref. 5, as

$$G_{\alpha\beta}(\mathbf{n}, z) = \hat{p}(\mathbf{n}, z) - \hat{p}(\mathbf{n}+\mathbf{e}_\alpha, z) - \hat{p}(\mathbf{n}-\mathbf{e}_\beta, z) + \hat{p}(\mathbf{n}+\mathbf{e}_\alpha-\mathbf{e}_\beta, z) \tag{3.1}$$

with

$$\hat{p}(\mathbf{n}, z) \equiv \hat{p}_d(\mathbf{n}, z) = \int_{\mathbf{q}} \frac{\exp(-i\mathbf{q}\mathbf{n})}{z+\omega(\mathbf{q})} \tag{3.2}$$

the Laplace-transformed probability of a displacement $\mathbf{n}$ on a uniform lattice. We will omit the subscript d unless the validity of the expressions is restricted to the specific choice of d, in fact being 2 or 3 in this paper.

By multiplying the integrand on the rhs of (3.2) with $z+\omega(q)$, it is straightforward to derive the recursion relations given below (see Morita[15]). For the square lattice we have [write $\mathbf{n}=(l, m)$]

$$\begin{aligned} 4(1+z)\,\hat{p}_2(l, m, z) = {} & 4\delta_{l0}\,\delta_{m0} + \hat{p}_2(l-1, m, z) + \hat{p}_2(l+1, m, z) \\ & + \hat{p}_2(l, m-1, z) + \hat{p}_2(l, m+1, z) \end{aligned} \tag{3.3a}$$

and for the simple cubic lattice [write $\mathbf{n}=(l, m, n)$]

$$\begin{aligned} 6(1+z)\,\hat{p}_3(l, m, n, z) = {} & 6\delta_{l0}\delta_{m0}\delta_{n0} + \hat{p}_3(l-1, m, n, z) + \hat{p}_3(l+1, m, n, z) \\ & + \hat{p}_3(l, m-1, n, z) + \hat{p}_3(l, m+1, n, z) \\ & + \hat{p}_3(l, m, n-1, z) + \hat{p}_3(l, m, n+1, z) \end{aligned} \tag{3.3b}$$

These relations can also be regarded as the defining equations for the $\hat{p}(\mathbf{n}, z)$. Together with the invariance of $\hat{p}_2(l, m, z)$ and $\hat{p}_3(l, m, n, z)$ under permutation of the indices l, m, n, and reflection of each index with respect to its origin, it is possible to derive symmetry relations for these $\hat{p}(\mathbf{n}, z)$, which, as a consequence, only have to be calculated for a restricted region of $\mathbf{n}$-space. The symmetries of the $\hat{p}$'s induce, of course, symmetries in the $G_{\alpha\beta}$ and the $R_{\alpha\beta}$, which can be used to check the numerical code.

The scheme for computing the $\hat{p}(\mathbf{n}, z)$ is described in detail in the Appendix; here, we present an outline. First we consider the 2D square lattice. The calculation requires the evaluation of complete elliptic integrals of the first and second kind. These give, in the right combinations, the $\hat{p}_2(0, 0, z)$ and $\hat{p}_2(1, 1, z)$. From these two quantities, the whole diagonal $\hat{p}_2(l, l, z)$ is calculated using an additional recurrence relation discussed in the Appendix. Next, the 2D recurrence relations (3.3a) are manipulated in such a way that they generate the $\hat{p}_2(l, m, z)$ for general l and m. Further, it is shown in the Appendix that we can calculate the whole 3D lattice from the knowledge of the data on a plane. The data on the $n=0$ plane follow from the 2D case as

$$\begin{aligned}
&\hat{p}_3(l, m, 0, z) \\
&\quad = \frac{1}{\pi^3}\int_0^\pi\int_0^\pi\int_0^\pi \frac{\cos lu \cos mv \, du \, dv \, dw}{1 + z - \frac{1}{3}(\cos u + \cos v + \cos w)} \\
&\quad = \frac{3}{2\pi}\int_0^\pi dw \, \frac{1}{\pi^2}\int_0^\pi\int_0^\pi \frac{\cos lu \cos mv \, du \, dv}{\frac{3}{2}(1 + z - \frac{1}{3}\cos w) - \frac{1}{2}(\cos u + \cos v)} \\
&\quad = \frac{3}{2\pi}\int_0^\pi dw \, \hat{p}_2\left(l, m, \frac{3}{2}z + \frac{1}{2}(1 - \cos w)\right)
\end{aligned} \tag{3.4}$$

Note that $\hat{p}_3(0, 0, 0, z)$ is the simple cubic lattice Green's function. Finally, making use of (3.3b), we generate the $\hat{p}_3(l, m, n, z)$ for arbitrary lattice vector $\mathbf{n}$.

4. STATIC DIFFUSION COEFFICIENT

In the previous sections we gave expressions for the Laplace-transformed VACF: $\Phi(z)$. The quantity that is calculated most easily following the lines of the previous sections is the static diffusion coefficient $D = D(\infty)$ [cf. (2.1)], which follows by taking $D = \Phi(z = 0)$. [Note that $\Phi(i\omega)$ is the frequency-dependent diffusion coefficient.] Thus, in order to obtain values for the diffusion coefficient, we have to evaluate (2.16) for $z = 0$. From

(2.13) and (2.12) we easily find $J(0)=1/d$ and $T(0)=b/2(d-b)$. We write the diffusion coefficient as

$$D(c)=D_0(1+\alpha_1 c+\alpha_2 c^2+\cdots) \tag{4.1}$$

where $D_0=1/2d$, the diffusion coefficient of the pure lattice, and

$$\alpha_1=-\frac{db}{d-b}$$

$$\alpha_2=-\frac{db}{d-b}\left[-\frac{db(1-b)}{(d-b)^2}\right.$$

$$\left.+\sum_{n\neq 0}\frac{R_{xx}^3(\mathbf{n},0)}{1-R_{xx}(\mathbf{n},0)}+(d-1)\sum_{\mathbf{n}}\frac{R_{xy}^4(\mathbf{n},0)}{1-R_{xy}^2(\mathbf{n},0)}\right] \tag{4.2}$$

For the explicit evaluation of the $O(c^2)$ terms for the 2D square lattice we refer to Ref. 5. Here, we are concerned with the 3D simple cubic case. In order to calculate the diffusion coefficient for three dimensions, we need the R_{xx} and R_{xy} for $z=0$, which involve the calculation of $\hat{p}_3(\mathbf{n}, 0)$ for arbitrary lattice vector $\mathbf{n}$. From (3.4) it is seen that this leads to the integration of the corresponding values of $\hat{p}_2(\mathbf{n}, z)$ for z varying from 0 to 1. The problem that arises here is that the $\hat{p}_2(\mathbf{n}, z)$ show logarithmic singularities near $z=0$. These originate from the behavior of the complete elliptic integral of the first kind near argument unity. To improve numerical accuracy we subtract the singular term from the integrand, evaluate it analytically, and add the result to the regular part afterward. The resulting values for $\hat{p}_3(l, m, 0)$ are tabulated in Table I. The values we obtain for $\hat{p}_3(0, 0, 0)$, $\hat{p}_3(1, 0, 0)$, $\hat{p}_3(1, 1, 0)$, and $\hat{p}_3(1, 1, 1)$ are in agreement (for all decimals given) with those given by Montet[16] and Watson.[17]

Proceeding in this way, we are able to evaluate the lattice sums in (4.2) using (2.14), (3.1), and (3.3b), giving the diffusion coefficient to quadratic order in the impurity concentration c. Finally, we can use the symmetry relation (2.5) to obtain the diffusion coefficient for c near unity, which requires the same calculations, but now for a value of b given by

$$b'=1-\sigma'=1-\frac{1}{\sigma}=1-\frac{1}{1-b}=\frac{-b}{1-b}$$

which is negative.

For later comparison of these results with the effective medium approximation we quote the relation from which the EMA values are calculated[6]:

$$(d-1)\psi^2+(2-d-b+cdb)\psi-1+b=0 \tag{4.3}$$

where $\psi = D(c)/D_0 = 2dD(c)$. The solution of this EMA equation for $d=2$ obeys the relation

$$\psi(c)\,\psi(1-c) = \sigma \tag{4.4}$$

following from the self-duality of the 2D square lattice bond problem.[19] For $c = 1/2$ this relation provides the exact result $\psi(1/2) = \sqrt{\sigma}$.

Further, Golden and Papanicolaou[20] calculated rigorous upper and lower bounds for the dielectric constant of a random mixture of dielectrics. These bounds also apply to the static diffusion coefficient studied here and are expressed as

$$\sigma M(1-c,\, 1/\sigma) \leqslant \psi(c,\, \sigma) \leqslant M(c,\, \sigma) \tag{4.5}$$

where [see Ref. 5, Eq. (4.12)]

$$M(c,\, \sigma) = 1 - \frac{bcd}{d - b(1-c)} \tag{4.6}$$

with $\psi \equiv D(c)/D_0 = 2dD(c)$ and $\sigma = 1 - b$.

Table I. Laplace-Transformed Probability of Displacement, or Green's Functions for the Simple Cubic Lattice: Values for $n=0$ and $z=0$[a]

m/l	0	1	2	3	4
5					
4					0.08427163
3				0.11228871	0.09539360
2			0.16833102	0.13245105	0.10705577
1		0.33114860	0.21558961	0.15313888	0.11713046
0	1.51638606	0.51638606	0.25733588	0.16527076	0.12173317
m/l	5	6	7	8	9
10					
9					0.03749653
8				0.04218216	0.03963500
7			0.04820203	0.04489430	0.04186254
6		0.05622468	0.05175681	0.04772922	0.04413563
5	0.06744918	0.06108567	0.05548385	0.05061019	0.04638613
4	0.07449474	0.06619578	0.05923929	0.05341530	0.04851774
3	0.08190985	0.07125597	0.06278699	0.05597097	0.05040631
2	0.08897732	0.07575721	0.06579001	0.05805805	0.05190865
1	0.09442927	0.07898507	0.06784389	0.05944131	0.05288310
0	0.09660640	0.08018811	0.06858197	0.05992815	0.05322168

[a] $\hat{p}$ is symmetric under permutation of l, m, and n. For comparison with Montet we also give $\hat{p}_3(1, 1, 1) = 0.26147013$.

It will be shown that these bounds, the EMA theory, and the density expansions are all in close agreement.

5. VELOCITY AUTOCORRELATION FUNCTION

The next problem we shall discuss in this paper is the calculation of the velocity autocorrelation function (VACF) and the time-dependent diffusion coefficient up to $O(c^2)$.

The way to obtain these quantities from the results reported in Sections 2 and 3 is by performing the Laplace inversion of the Laplace-transformed VACF $\Phi(z)$ given by (2.16).

One of the basic quantities that possesses the kind of singularities we have to deal with is $J(z)$ given in (2.13). Obviously $J(z)$ falls off as $1/z$ for $|z| \to \infty$. As $\omega(q)$ varies from 0 to 2, it is clear that $J(z)$ shows a branch cut on the real axis from -2 to 0. Subsequently we shall need the values of $J(z)$ just below this branch cut. For a discussion of the behavior of $J(z)$ in this region of the complex z plane we refer to the Appendix.

The Laplace inversion for a function $\hat{f}(z)$ is carried out by taking the integral

$$f(t) = \mathscr{L}^{-1}(\hat{f}(z)) = \frac{1}{2\pi i} \int_{\eta - i\infty}^{\eta + i\infty} dz\, e^{zt} \hat{f}(z) \tag{5.1}$$

Apart from the constant term $T(\infty)$ in $T(z)$, all terms in (2.16) decay sufficiently rapidly for $|z| \to \infty$ so the contour can be closed in the left half of the complex z plane. For the present, we assume that there are, outside the branch cut, no further poles present. This is certainly the case for b values greater than zero.[13] Now, the contour is equivalent to the contour that goes anticlockwise just below and just above the branch cut. The functions we have to invert are real functions of a complex argument, so they obey the relation $\hat{f}(x + i0) = \hat{f}^*(x - i0)$, where the asterisk means complex conjugation. Thus, we can write the Laplace inversion as

$$\begin{aligned} f(t) &= \frac{1}{2\pi i} \int_{-2}^{0} dx\, e^{xt} [\hat{f}(x - i0) - \hat{f}(x + i0)] \\ &= \frac{1}{\pi} \int_{0}^{2} dx\, e^{-xt} \operatorname{Im}[\hat{f}_-(-x)] \end{aligned}$$

where $f_-(-x) \equiv f(-x - i0)$. Using this formula, we can calculate various inversions. Consider first $T(z)$ in (2.16). The term $T(z) - T(\infty)$ falls off as $1/|z|$, while the constant $T(\infty) = b/2d$ leads to $(b/2d)\, \delta_+(t)$. Thus,

$$\mathscr{L}^{-1}(T) = \frac{b}{2d}\delta_+(t) + \frac{b}{2d}\mathscr{L}^{-1}\left(\frac{bJ}{1-bJ}\right)$$

$$= \frac{b}{2d}\delta_+(t) + \frac{b}{2d}\frac{1}{\pi}\int_0^2 dx\, e^{-xt}\frac{bJ_I}{|1-bJ|^2} \tag{5.2}$$

where $J_-(-x) \equiv J(-x-i0) \equiv J_R(x) + iJ_I(x)$.

In a similar fashion, we find

$$\mathscr{L}^{-1}(J^3) = \frac{1}{\pi}\int_0^2 dx\, e^{-xt}\,\mathrm{Im}\, J_-^3(-x)$$

$$= \frac{1}{\pi}\int_0^2 dx\, e^{-xt}(3J_R^2 - J_I^2)\, J_I \tag{5.3}$$

$$\mathscr{L}^{-1}(T^2J) = \left(\frac{b}{2d}\right)^2 \mathscr{L}^{-1}\left(\frac{J}{(1-bJ)^2}\right)$$

$$= \left(\frac{b}{2d}\right)^2 \frac{1}{\pi}\int_0^2 dx\, e^{-xt} J_I \frac{1-|bJ|^2}{|1-bJ|^4} \tag{5.4}$$

$$\mathscr{L}^{-1}(T^3J^2) = \frac{1}{b}\left(\frac{b}{2d}\right)^3 \frac{1}{\pi}\int_0^2 dx\, e^{-xt} J_I \frac{2bJ_R - 3|bJ|^2 + |bJ|^4}{|1-bJ|^6} \tag{5.5}$$

Now we are left, apart from the lattice sums in (2.16), with the term T^3I that has to be inverted. Because we know the structure of $J(z)$ very well, we would like to express $\mathscr{L}^{-1}(T^3I)$ in terms of J. This can be done in the following way [note that $dJ(z)/dz = -dJ(-x)/dx$]:

$$\mathscr{L}^{-1}(T^3I) = \left(\frac{b}{2d}\right)^3 \mathrm{Im}\,\frac{1}{\pi}\int_0^2 dx\, e^{-xt}\frac{J_- + x\, dJ_-/dx}{(1-bJ_-)^3}$$

$$= \frac{1}{2b}\left(\frac{b}{2d}\right)^3 \mathrm{Im}\,\frac{1}{\pi}\int_0^2 dx\, e^{-xt}\left\{\frac{3bJ_- - 1}{(1-bJ_-)^3}\right.$$

$$\left. + \frac{d}{dx}\left(\frac{x}{(1-bJ_-)^2}\right)\right\}$$

which, via partial integration, yields

$$\mathscr{L}^{-1}(T^3I) = \left(\frac{b}{2d}\right)^3 \frac{1}{\pi}\int_0^2 dx\, e^{-xt} J_I$$

$$\times\left(\frac{|bJ|^2(3bJ_R - 4) + 3bJ_R - 2(bJ_R)^2}{|1-bJ|^6} + \frac{xt(1-bJ_R)}{|1-bJ|^4}\right) \tag{5.6}$$

With knowledge of J_R and J_I along the branch cut, the expressions (5.3)–(5.6) can be integrated numerically. The expressions involved in the inversion of the lattice sums in (2.16) are quite lengthy and do not contain essential differences with respect to the foregoing and we will not write them down here.

The way in which we perform the integrations is the following. Using a Gaussian quadrature formula, we have to calculate the integrands on the mesh of points $x \in \langle 0, 2 \rangle$ prescribed by the method. For each x we generate the $\hat{p}(\mathbf{n}, -x - i0)$ on the entire lattice; in fact, we obtain convergence well within ten lattice distances from the origin. In doing this, we use the several recursion formulas given in the Appendix. From these $\hat{p}(\mathbf{n}, -x - i0)$ we calculate the G, J, T, and R, using (3.1), (2.13), (2.10), (2.12), and (2.14). Continuing, we evaluate the imaginary parts of the analytically obtained summations [cf. (5.2)–(5.6)] and of the summands $TR_{xx}^3/(1-R_{xx})$ and $TR_{xy}^4/(1-R_{xy}^2)$. Summing up all these numbers multiplied by their appropriate Gaussian weights and performing the lattice summations leads to the final result. Note that the "analytical" terms (5.2)–(5.6) only require the value of $\hat{p}(\mathbf{n}, -x - i0)$ at the origin $\mathbf{n} = 0$ of the lattice.

The integrands in (5.2)–(5.6) have the same general form $e^{-xt}h(x)$, where $h(x)$ is some real-valued function of x. This property enables us to find a different representation of these integrals. We first use the identity

$$\frac{1}{\omega(\mathbf{q}) - x - i\varepsilon} = \mathscr{P}\left[\frac{1}{\omega(\mathbf{q}) - x}\right] + \pi i\, \delta(\omega(\mathbf{q}) - x) \tag{5.7}$$

where $\varepsilon \downarrow 0$ and $\mathscr{P}$ denotes the principal value. We observe that

$$J_I(x) = \frac{1}{d} \operatorname{Im} \int_{\mathbf{q}} \frac{\omega(\mathbf{q})}{\omega(\mathbf{q}) - x - i\varepsilon} = \frac{\pi}{d} \int_{\mathbf{q}} \omega(\mathbf{q})\, \delta(\omega(\mathbf{q}) - x) \tag{5.8}$$

Consequently, we find the integral representation

$$\begin{aligned} &\frac{1}{\pi} \int_0^2 dx\, e^{-xt} J_I(x)\, h(x) \\ &\quad = \frac{1}{d} \int_{\mathbf{q}} \omega(\mathbf{q}) \int_0^2 dx\, e^{-xt} h(x)\, \delta(\omega(\mathbf{q}) - x) \\ &\quad = \frac{1}{d} \int_{\mathbf{q}} \omega(\mathbf{q})\, e^{-\omega(\mathbf{q})t} h(\omega(\mathbf{q})) \end{aligned} \tag{5.9}$$

where the second equality follows from the range of $\omega(\mathbf{q})$: $[0, 2]$. For the

inversion of J, i.e., $h \equiv 1$, the result is simply equivalent to the replacement of $1/(z+\omega)$ in (2.13) by its Laplace invert $e^{-\omega t}$. The advantage of this formulation is that the integrand in (5.7), at least for the inversion of a single factor J, does not contain singularities, which implies more stability in case of a numerical evaluation, as opposed to the integrals (5.2)–(5.6), which still involve the function $J(z)$. The Laplace inversion of J and $\hat{p}(\mathbf{n})$ can also be expressed in terms of Bessel functions (see Ref. 21, Eq. [9.1.21]). However, the inversion of powers of J or $\hat{p}(\mathbf{n})$ becomes very complicated, if not impossible, using these Bessel functions.

Now we have two methods, integration schemes, for performing the calculations. Both methods, i.e., "contour integration" and "1BZ integration," have been programmed, using a Gaussian quadrature method. The 1BZ formalism looks more attractive, because the inversion of J can be performed more accurately, the integrand [cf. (5.9)] containing no singularities. In fact, compared with the "contour" formalism, each integrand looks "nicer" by a factor J. However, in the 1BZ integrations we have to use much more integration points to obtain an equally dense covering of the integration interval, which is two-dimensional for the square lattice and three-dimensional for the simple cubic lattice. This leads to a large increase in computer time needed, compared with the "contour" method. Moreover, we have not been able to apply the 1BZ method to the lattice sums in a way that can be handled numerically in an elegant manner (e.g., using recursion formulas); it would involve separate calculations for each lattice site.

The various components in two dimensions show discontinuities and/or singularities at $z = -1$ and similarly in three dimensions at $z = -4/3$ and $-2/3$ (see Appendix). Therefore, the integration intervals have been split up. This is easy for the contour integration, but also possible for the 1BZ integration. The reader can verify the latter by considering domain and range of the function $\omega(\mathbf{q})$.

6. TIME-DEPENDENT DIFFUSION COEFFICIENT

Having set up the numerical code for the calculation of the velocity autocorrelation function (VACF) for all values of the time t, it is not difficult to adjust the code for calculating the time-dependent diffusion coefficient as well. This is most easily done after noting that the time dependence of the expressions in Section 5 is quite simple. The expressions have the form

$$\int [f(x) + txg(x)]\, e^{-xt}\, dx \tag{6.1}$$

If we integrate this from 0 to t over time according to Eq. (2.1), interchanging the order of integration, we simply obtain

$$\int \left[f(x) \frac{1-e^{-xt}}{x} + g(x) \frac{1-e^{-xt}(1+xt)}{x} \right] dx \tag{6.2}$$

The changes needed are easily implemented in the numerical code. The only thing we have to keep in mind is that $\mathscr{L}^{-1}(T)$ contains a delta function $(b/2d)\,\delta(t)$. This term, when integrated from 0 to t, yields a constant contribution $-b/2d$ to the $O(c)$ part of the diffusion coefficient.

7. RESULTS AND DISCUSSION

In this paper we have given numerical data obtained from the density expansion formalism developed for bond percolation models.[2,4,5] We have calculated the velocity autocorrelation function (VACF) and the time-dependent diffusion coefficient using the expressions given by Ernst and Van Velthoven[5] and quoted in Section 2 of this paper. More specifically, we have performed calculations for the $O(c^2)$ terms of these two quantities, c being the concentration of impurity bonds.

To start with the static diffusion coefficient, the following has been done. We calculated the density expansions for several values of the conductivity of the impurity bonds σ $(=1-b)$. The low-density (small-c) as well as the high-density [small-$(1-c)$] expansions up to second order have been evaluated, i.e., $\psi(c) = 1 + \alpha_1 c + \alpha_2 c^2$ and $\psi(c) = \sigma[1 + \alpha_1'(1-c) + \alpha_2'(1-c)^2]$. The coefficients b $(=1-\sigma)$, α_1, α_2, α_1', and α_2' are tabulated in Table II. Values for the 2D case were already given in Ref. 5. For the percolation case in three dimensions the coefficient of c^2 is very small (-0.0108). Please note that it is smaller than the preliminary value of -0.0162 reported earlier.[18] Moreover, it is negative, as in the 2D case, and leads to a value of the percolation threshold smaller than the EMA value $c_p = 2/3$, which is the same as follows from the linear c expansion. Note that Monte Carlo calculations give a percolation concentration of $c_p \simeq 0.753$.[16] For $b = 0.99$ the $O(c^2)$ is still negative (-0.1489) in the 2D case, while it is slightly positive (0.001058) for the 3D case. For the b values of 0.9 and smaller (higher conductivity of impurity bonds) all $O(c^2)$ coefficients are positive.

The only experimental data (computer simulations) available are for the percolation case $(b = 1)$, where the agreement between the results from low-density theory and finite-density computer simulations is surprisingly

Table II. Numerical Values for the Static Diffusion Coefficient [cf. Eq. (4.1)] for the Three-Dimensional Bond Model[a]

b	α_1	α_2	b'	α_1'	α_2'
1.0	−1.5	−0.010807			
0.99	−1.47761	0.001058	−99.0	2.911765	9.354451
0.9	−1.28571	0.074904	−9.0	2.25	4.504801
0.8	−1.0909	0.107144	−4.0	1.714286	2.175755
0.7	−0.91304	0.108634	−2.333	1.3125	1.098392
0.6	−0.75	0.093873	−1.5	1.0	0.561745
0.5	−0.60000	0.072114	−1.0	0.750000	0.282933
0.4	−0.461538	0.049218	−0.666	0.545455	0.135646
0.3	−0.333333	0.028828	−0.4286	0.375000	0.058674
0.2	−0.214286	0.013124	−0.25	0.230769	0.020493

[a] We must emphasize that the value −0.0162 reported in Ref. 17 for α_2 ($b = 1.0$) was incorrect.

good. In the site models,[2] the agreement between theory and simulations is poor to $O(c)$ and satisfactory to $O(c^2)$.

From the data obtained from our density expansion we can construct a smooth interpolation between the low- and high-density expansions using the technique of Padé approximants. As we have six parameters, $D(c=0)$, $D(c=1)$, α_1, α_2, α_1', and α_2', available, we can construct the $[n, m]$ approximants with $n+m=5$, where n and m are the powers of the polynomials in numerator and denominator, respectively. The values of these polynomials at $c=0$ are taken equal to 1, because $\psi(0)=1$. We chose to calculate the [4, 1], [3, 2], and [2, 3] Padé approximants (see Fig. 1).

The EMA provides values of the diffusion coefficient [cf. Eq. (4.3)] that show a smooth transition from the small-c to the large-c domain. The slopes of these curves at $c=0$ and $c=1$ are the same as in the density expansion (4.2). In addition, for the 2D case the EMA follows the self-duality relation (4.4) and, by consequence, is exact for $c=1/2$: $\psi(1/2)=D(1/2)/D_0=\sqrt{\sigma}$ (see Refs. 5 and 19).

The same features are found in a renormalization group treatment of this 2D problem,[10] showing that RG calculations yield very accurate results for the static transport properties, at least for the 2D square bond models. Results for frequency-dependent transport properties, using RG calculations, do not seem to be available in the literature.

For most b values the different Padé curves and the EMA curve are nearly indistinguishable. The strongest disagreement between the different approximants occurs for b values near unity. We took an extreme b value

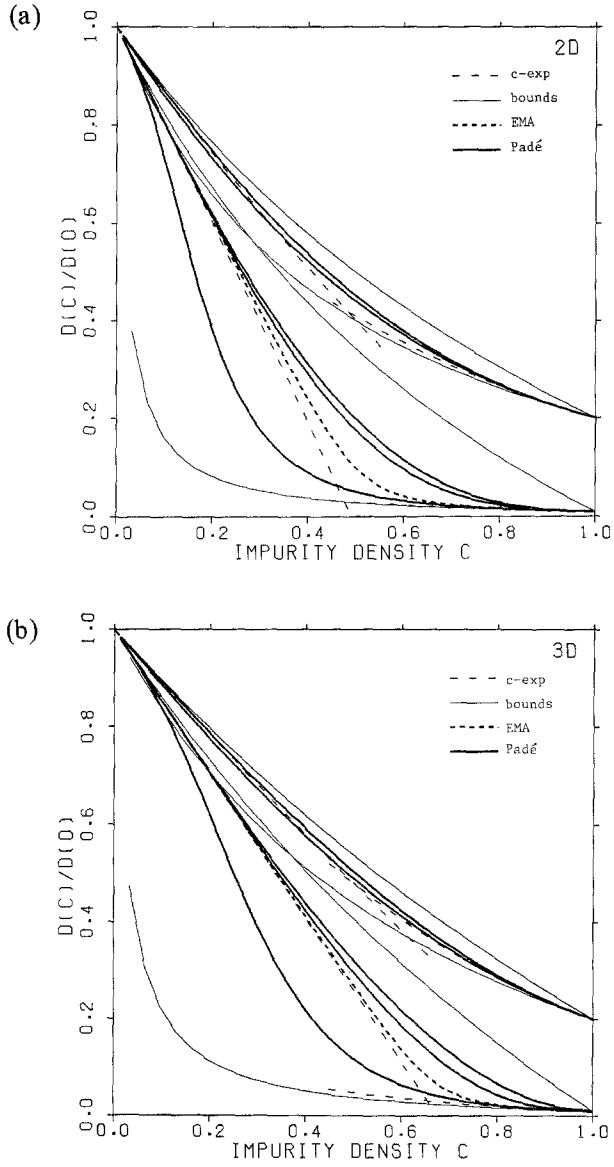

Fig. 1. Static diffusion coefficient. Comparison of different approximations for $b = 0.99$ and $b = 0.8$, where $D(1)/D(0) = 1 - b$. Rigorous upper and lower bounds (thin, solid lines) high and low-density expansions (thin, dashed lines) EMA (heavy, dashed line, merged with Padé curves for $b = 0.8$), and the [4, 1], [3, 2] and [2, 3] Padé approximants (heavy, solid lines). (a) 2D, (b) 3D. Parts of (a) and (b) magnified by a factor of five, showing the EMA and Padé curves for $b = 0.8$. Left to right: the [2, 3], [4, 1], and [3, 2] approximants.

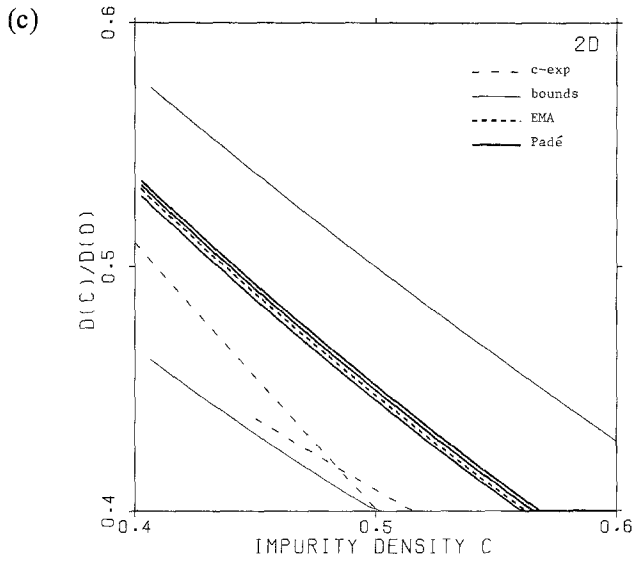

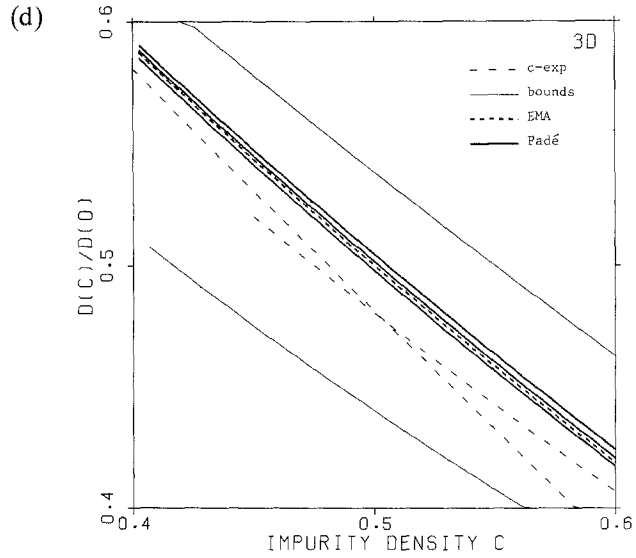

Fig. 1 (*continued*)

of 0.99 to show the differences. In Fig. 1 these results are shown together with those for $b = 0.8$, where everything is in close agreement. We plotted the density expansions [the curves representing the small-c and small-$(1-c)$ expansions have been cut off from the right and the left, respectively], the EMA curves, the Padé approximants, and the rigorous bounds described by Eqs (4.5)–(4.6).

It is seen that the density expansions and the EMA curves lie well within the bounds. Even the intersections of high- and low-density curves (which are not to be considered as a good estimate of ψ) obey these bounds. For $b = 0.8$ the Padé curves can hardly be distinguished from each other and the EMA result. For this reason only the smallest and highest Padé approximants are plotted; the EMA and the other approximant lie in between these curves, as can be seen in Figs. 1c and 1d, containing magnified graphs for $b = 0.8$. For two dimensions we have the additional check that $\psi(1/2) = \sqrt{\sigma}$. The EMA gives this exact value, 0.447, while the [4, 1], [3, 2], and [2, 3] Padé approximants give 0.450, 0.440, and 0.445, respectively. The [2, 3] approximant could not generally be taken as the "best," as could be seen from the $b = 0.99$ case, where we have ($\sqrt{\sigma} = 0.1$) 0.194, 0.176, and 0.051, respectively.

In Fig. 2 we present an overview of the available data for the static diffusion coefficient for the models with bond disorder, the square lattice in Fig. 2a, the simple cubic in Fig. 2b. Instead of displaying the density expansions and the Padé approximations as well, it suffices to show the EMA curves, which describe the theory reasonably well over the whole range of c values. In Fig. 2b we also include Kirkpatrick's data,[6] obtained from simulation of the 3D percolation model (the $b = 1$ model). (For a comparison with simulations in two dimensions we refer to Ref. 4.) Although these data refer to $b = 1$, they seem to be described in a better way by our $b = 0.99$ curve. Here we recall that EMA gives a poor prediction of the 3D percolation threshold and is bound to be in error for densities in the vicinity of this percolation threshold ($c_p \simeq 0.753$).

The major part of the effort was put into the calculation of the time-dependent diffusion coefficient $D(t)$ and the velocity autocorrelation function VACF(t) (cf. Sections 5 and 6 of this paper). The calculations have been performed for several different values of the parameter b. The most interesting behavior is, as can be expected, shown by the percolation case $b = 1$. The results for this case are shown in Figs. 3a and 4a (diffusion coefficient) and Figs. 3b and 4b (VACF). The results for other b values are included in Tables III and IV. We considered 90 time points, of which every third is given in the tables. We plotted and tabulated the quantities $\bar{\alpha}_1(t)[= \alpha_1(t) + b$, to separate out the Enskog part], $\alpha_2(t)$, $\beta_1(t)$, and $\beta_2(t)$ as they appear in

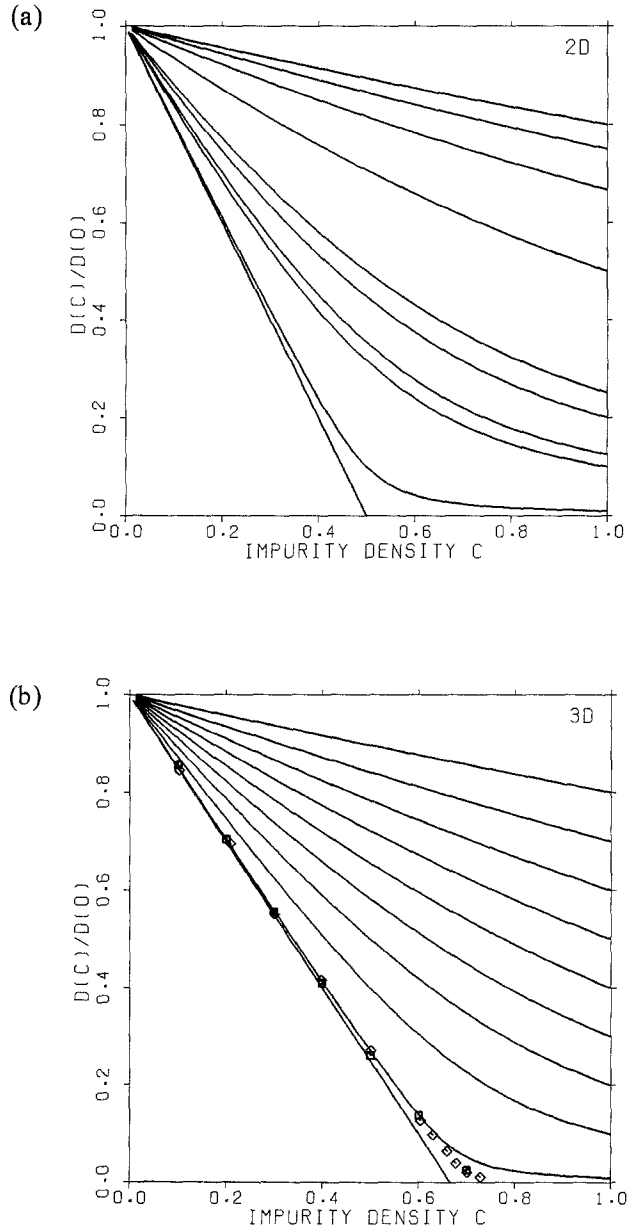

Fig. 2. EMA results for the static diffusion coefficient. (a) 2D case for $b = 1$, 99/100, 7/8, 4/5, 3/4, 1/2, 1/3, 1/4, and 1/5. (b) 3D case for $b = 1.0$, 0.99, 0.9, 0.8, 0.7, 0.6, 0.5, 0.4, 0.3, and 0.2. The squares and tilted squares represent simulation data given by Kirkpatrick.[6]

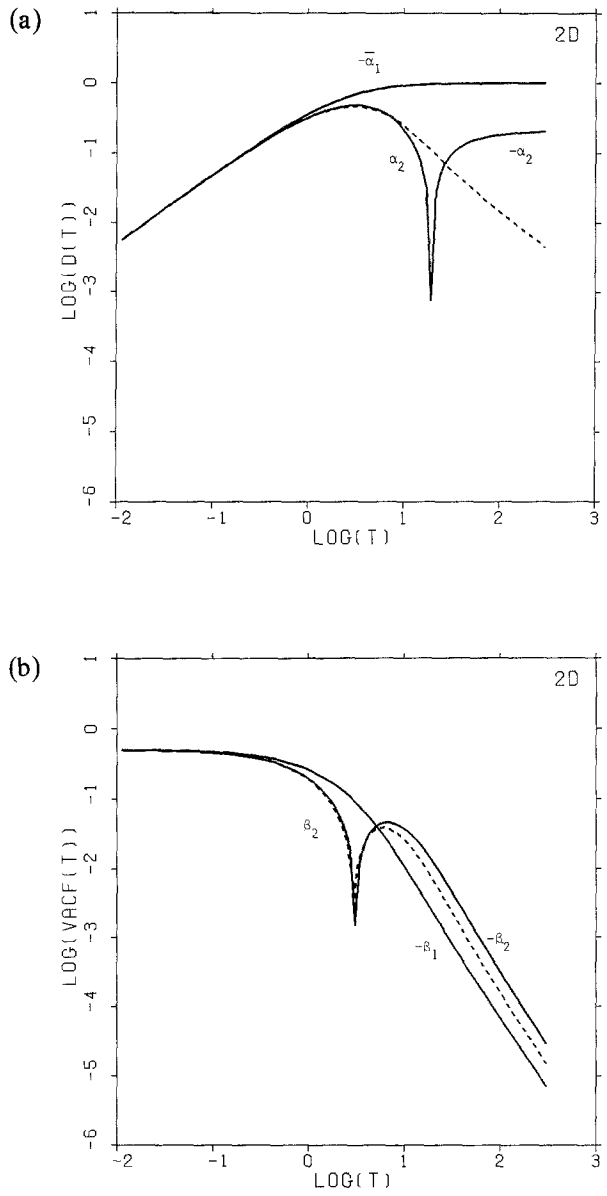

Fig. 3. (a) Time dependence of $D(t)$ contributions in 2D bond percolation ($b = 1$) to $O(c)$ and $O(c^2)$, as defined in Eq. (7.1). The dashed line represents the EMA part of $\alpha_2(t)$. Cusps indicate changes in sign. (b) Contributions to the velocity autocorrelation function (VACF) for 2D bond percolation ($b = 1$) to $O(c)$ and $O(c^2)$ as defined in Eq. (7.1). The EMA contribution to $\beta_2(t)$ is represented by a dashed line.

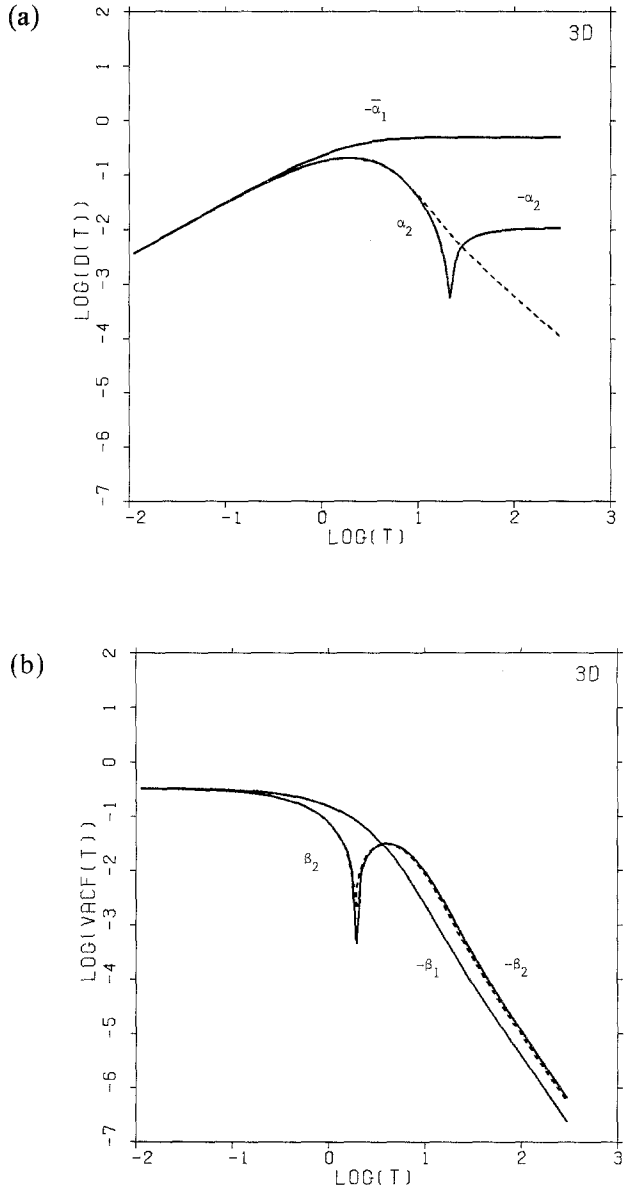

Fig. 4. (a) Time dependence of $D(t)$ contributions in 3D bond percolation ($b=1$) to $O(c)$ and $O(c^2)$, as defined in Eq. (7.1). The dashed line represents the EMA part of $\alpha_2(t)$. Cusps indicate changes in sign. (b) Contributions to the velocity autocorrelation function (VACF) for 3D bond percolation ($b=1$) to $O(c)$ and $O(c^2)$ as defined in Eq. (7.1). The EMA contribution to $\beta_2(t)$ is represented by a dashed line.

Table III. Results for the 2D Bond Model: Coefficients of Linear and Quadratic Terms beyond Enskog (Diffusion) and Initial Delta Function (VACE)[a]

	Time-dependent diffusion coefficient						Velocity autocorrelation function					
	$b=0.6$		$b=0.8$		$b=1.0$		$b=0.6$		$b=0.8$		$b=1.0$	
t	$-\tilde{\alpha}_1$	α_2	$-\tilde{\alpha}_1$	α_2	$-\tilde{\alpha}_1$	α_2	$-\beta_1$	β_2	$-\beta_1$	β_2	$-\beta_1$	β_2
0.014	.2521E-2	.2519E-2	.4485E-2	.4480E-2	.7013E-2	.7005E-2	.1776	.1772	.3162	.3155	.4948	.4933
0.020	.3545E-2	.3540E-2	.6309E-2	.6298E-2	.9868E-2	.9849E-2	.1766	.1761	.3147	.3136	.4926	.4905
0.028	.4980E-2	.4970E-2	.8866E-2	.8843E-2	.1387E-1	.1383E-1	.1753	.1746	.3125	.3109	.4896	.4865
0.040	.6984E-2	.6965E-2	.1244E-1	.1240E-1	.1948E-1	.1939E-1	.1734	.1724	.3095	.3072	.4855	.4810
0.056	.9774E-2	.9735E-2	.1742E-1	.1733E-1	.2730E-1	.2713E-1	.1708	.1694	.3053	.3021	.4797	.4733
0.079	.1364E-1	.1356E-1	.2434E-1	.2415E-1	.3817E-1	.3782E-1	.1671	.1652	.2995	.2950	.4716	.4627
0.111	.1894E-1	.1879E-1	.3386E-1	.3351E-1	.5319E-1	.5250E-1	.1622	.1596	.2916	.2854	.4606	.4483
0.156	.2616E-1	.2588E-1	.4686E-1	.4618E-1	.7379E-1	.7243E-1	.1555	.1521	.2808	.2725	.4457	.4288
0.220	.3584E-1	.3530E-1	.6440E-1	.6308E-1	.1017	.9907E-1	.1467	.1422	.2665	.2555	.4257	.4030
0.311	.4856E-1	.4757E-1	.8763E-1	.8516E-1	.1390	.1339	.1352	.1296	.2479	.2336	.3995	.3695
0.438	.6485E-1	.6306E-1	.1177	.1131	.1877	.1783	.1208	.1140	.2243	.2065	.3661	.3274
0.618	.8496E-1	.8185E-1	.1553	.1472	.2497	.2324	.1036	.9579E-1	.1957	.1743	.3251	.2766
0.871	.1086	.1035	.2006	.1866	.3257	.2948	.8408E-1	.7578E-1	.1628	.1383	.2770	.2181
1.228	.1348	.1267	.2521	.2289	.4148	.3608	.6370E-1	.5552E-1	.1274	.1008	.2242	.1549
1.732	.1617	.1496	.3069	.2701	.5133	.4219	.4433E-1	.3691E-1	.9260E-1	.6523E-1	.1701	.9138E-1
2.442	.1868	.1699	.3607	.3046	.6148	.4645	.2795E-1	.2172E-1	.6159E-1	.3495E-1	.1196	.3354E-1
3.444	.2080	.1855	.4088	.3272	.7113	.4728	.1583E-1	.1096E-1	.3710E-1	.1286E-1	.7699E-1	-.1181E-1
4.856	.2241	.1958	.4477	.3348	.7947	.4336	.8095E-2	.4616E-2	.2017E-1	.1720E-3	.4496E-1	-.3876E-1
6.847	.2352	.2014	.4762	.3292	.8603	.3460	.3838E-2	.1625E-2	.1002E-1	-.4407E-2	.2383E-1	-.4576E-1
9.655	.2426	.2041	.4956	.3164	.9074	.2266	.1762E-2	.5196E-3	.4690E-2	-.4245E-2	.1164E-1	-.3800E-1
13.614	.2473	.2053	.5082	.3028	.9390	.1036	.8131E-3	.1776E-3	.2152E-2	-.2667E-2	.5408E-2	-.2475E-1
19.197	.2504	.2059	.5164	.2920	.9595	.7496E-3	.3823E-3	.7210E-4	.9954E-3	-.1368E-2	.2473E-2	-.1342E-1
27.068	.2525	.2063	.5217	.2846	.9727	-.7312E-1	.1830E-3	.3351E-4	.4683E-3	-.6408E-3	.1141E-2	-.6448E-2
38.168	.2539	.2065	.5253	.2798	.9814	-.1216	.8874E-4	.1661E-4	.2240E-3	-.2920E-3	.5352E-3	-.2924E-2
53.819	.2549	.2067	.5278	.2767	.9872	-.1523	.4346E-4	.8418E-5	.1085E-3	-.1334E-3	.2554E-3	-.1310E-2
75.888	.2556	.2069	.5294	.2747	.9911	-.1718	.2144E-4	.4292E-5	.5310E-4	-.6182E-4	.1235E-3	-.5942E-3
107.006	.2560	.2069	.5306	.2734	.9938	-.1844	.1063E-4	.2192E-5	.2617E-4	-.2906E-4	.6035E-4	-.2745E-3
150.885	.2564	.2070	.5314	.2725	.9956	-.1927	.5290E-5	.1120E-5	.1297E-4	-.1385E-4	.2971E-4	-.1291E-3
212.757	.2566	.2071	.5320	.2719	.9969	-.1982	.2640E-5	.5712E-6	.6449E-5	-.6671E-5	.1471E-4	-.6169E-4
300.000	.2568	.2071	.5324	.2715	.9978	-.2020	.1320E-5	.2906E-6	.3217E-5	-.3246E-5	.7311E-5	-.2983E-4

[a] See also Eq. (7.1) and Figs. 3a and 3b.

Table IV. Results for the 3D Bond Model: Coefficients of Linear and Quadratic Terms beyond Enskog (Diffusion) and Initial Delta Function (VACE)[a]

	Time-dependent diffusion coefficient						Velocity autocorrelation function					
	$b=0.6$		$b=0.8$		$b=1.0$		$b=0.6$		$b=0.8$		$b=1.0$	
t	$-\bar{\alpha}_1$	α_2	$-\bar{\alpha}_1$	α_2	$-\bar{\alpha}_1$	α_2	$-\beta_1$	β_2	$-\beta_1$	β_2	$-\beta_1$	β_2
0.014	.1681E-2	.1677E-2	.2989E-2	.2981E-2	.4673E-2	.4656E-2	.1184	.1179	.2106	.2095	.3294	.3271
0.020	.2363E-2	.2356E-2	.4204E-2	.4187E-2	.6573E-2	.6540E-2	.1177	.1170	.2096	.2079	.3279	.3246
0.028	.3319E-2	.3306E-2	.5906E-2	.5874E-2	.9237E-2	.9172E-2	.1168	.1158	.2080	.2057	.3257	.3211
0.040	.4654E-2	.4628E-2	.8286E-2	.8221E-2	.1296E-1	.1283E-1	.1155	.1142	.2059	.2027	.3226	.3162
0.056	.6512E-2	.6459E-2	.1160E-1	.1147E-1	.1816E-1	.1790E-1	.1137	.1119	.2029	.1984	.3183	.3094
0.079	.9084E-2	.8980E-2	.1619E-1	.1594E-1	.2536E-1	.2487E-1	.1113	.1087	.1988	.1926	.3123	.3001
0.111	.1262E-1	.1241E-1	.2251E-1	.2202E-1	.3530E-1	.3433E-1	.1079	.1044	.1932	.1848	.3042	.2873
0.156	.1741E-1	.1702E-1	.3112E-1	.3018E-1	.4887E-1	.4700E-1	.1033	.9860E-1	.1857	.1742	.2931	.2703
0.220	.2384E-1	.2310E-1	.4269E-1	.4089E-1	.6718E-1	.6359E-1	.9730E-1	.9105E-1	.1755	.1603	.2783	.2478
0.311	.3227E-1	.3088E-1	.5794E-1	.5456E-1	.9144E-1	.8465E-1	.8945E-1	.8143E-1	.1623	.1426	.2590	.2189
0.438	.4303E-1	.4049E-1	.7755E-1	.7131E-1	.1228	.1102	.7959E-1	.6967E-1	.1457	.1209	.2343	.1833
0.618	.5623E-1	.5173E-1	.1018	.9067E-1	.1622	.1393	.6775E-1	.5605E-1	.1255	.9560E-1	.2042	.1414
0.871	.7163E-1	.6398E-1	.1306	.1112	.2093	.1690	.5435E-1	.4143E-1	.1023	.6829E-1	.1693	.9562E-1
1.228	.8839E-1	.7606E-1	.1625	.1305	.2627	.1945	.4034E-1	.2721E-1	.7765E-1	.4158E-1	.1314	.5004E-1
1.732	.1051	.8641E-1	.1952	.1452	.3187	.2087	.2713E-1	.1508E-1	.5379E-1	.1877E-1	.9377E-1	.1041E-1
2.442	.1201	.9364E-1	.2254	.1520	.3724	.2048	.1617E-1	.6407E-2	.3329E-1	.2758E-2	.6030E-1	-.1758E-1
3.444	.1319	.9717E-1	.2502	.1499	.4183	.1790	.8383E-2	.1527E-2	.1803E-1	-.5339E-2	.3420E-1	-.3057E-1
4.856	.1400	.9767E-1	.2679	.1406	.4526	.1352	.3746E-2	-.3341E-3	.8424E-2	-.6835E-2	.1678E-1	-.2964E-1
6.847	.1447	.9661E-1	.2787	.1288	.4747	.8507E-1	.1465E-2	-.5541E-3	.3405E-2	-.4825E-2	.7078E-2	-.2049E-1
9.655	.1472	.9541E-1	.2846	.1191	.4870	.4289E-1	.5291E-3	-.3052E-3	.1240E-2	-.2372E-2	.2627E-2	-.1051E-1
13.614	.1485	.9464E-1	.2876	.1131	.4933	.1597E-1	.1910E-3	-.1152E-3	.4393E-3	-.9003E-3	.9192E-3	-.4159E-2
19.197	.1492	.9426E-1	.2891	.1101	.4964	.2150E-2	.7214E-4	-.3841E-4	.1617E-3	-.3039E-3	.3286E-3	-.1400E-2
27.068	.1495	.9408E-1	.2899	.1087	.4980	-.4284E-2	.2839E-4	-.1323E-4	.6239E-4	-.1043E-3	.1237E-3	-.4622E-3
38.168	.1497	.9399E-1	.2903	.1080	.4989	-.7354E-2	.1146E-4	-.4846E-5	.2487E-4	-.3805E-4	.4853E-4	-.1623E-3
53.819	.1498	.9395E-1	.2906	.1076	.4993	-.8919E-2	.4699E-5	-.1857E-5	.1012E-4	-.1456E-4	.1954E-4	-.6059E-4
75.888	.1499	.9392E-1	.2907	.1074	.4996	-.9759E-2	.1947E-5	-.7338E-6	.4169E-5	-.5756E-5	.7999E-5	-.2357E-4
107.006	.1499	.9390E-1	.2908	.1073	.4998	-.1023E-1	.8121E-6	-.2960E-6	.1733E-5	-.2324E-5	.3309E-5	-.9421E-5
150.885	.1500	.9390E-1	.2908	.1072	.4999	-.1049E-1	.3403E-6	-.1212E-6	.7242E-6	-.9521E-6	.1379E-5	-.3833E-5
212.757	.1500	.9389E-1	.2909	.1072	.4999	-.1064E-1	.1430E-6	-.5012E-7	.3039E-6	-.3940E-6	.5774E-6	-.1579E-5
300.000	.1500	.9389E-1	.2909	.1072	.5000	-.1073E-1	.6025E-7	-.2088E-7	.1278E-6	-.1642E-6	.2426E-6	-.6557E-6

[a] See also Eq. (7.1) and Figs. 4a and 4b.

$$D(t)=\frac{1}{2d}\left[1-bc+\bar{\alpha}_1(t)\,c+\alpha_2(t)\,c^2\right]$$
$$\varphi(t)=\frac{1}{2d}\left[(1-bc)\,\delta_+(t)+\beta_1(t)\,c+\beta_2(t)\,c^2\right] \tag{7.1}$$

The reason for doing so is to facilitate the comparison of the static and time-dependent diffusion coefficients here and all present results with those obtained in the context of the effective medium theory.

The EMA contributions to $\alpha_2(t)$ and $\beta_2(t)$ (indicated by dashed lines in Figs. 3 and 4) are missing the contributions from the lattice sums in Eq. (2.16). These lattice sums account for dynamical events in which the RW crosses three or more times between two impurities. For more details we refer elsewhere.[22]

The use of logarithmic scales forced us to plot the absolute values of the quantities; thus, each zero appears as a cusp in the graph; the signs of the quantities are indicated in the figures. For the diffusion coefficient we exclude the Enskog or high-frequency part $bc/2d$ from the linear term to prevent the (log–log) graph from becoming virtually constant-valued.

The large-z and small-z behavior of $\Phi(z)$ [Eq. 2.16] can be studied analytically (see also Ref. 13), yielding the short-time and long-time asymptotics, respectively. We investigated the time scales on which the different terms in (2.16) assume their long-time asymptotic behavior. To do so, we start from the leading and subleading long-time tails of $(\mathscr{L}^{-1}J)(t)$ [cf. Eq. (2.13)]. After some lengthy, but straightforward calculations these yield the tails of the terms T, T^2J, T^3J^2, and T^3I.

We observe that in the 2D model the leading and subleading long-time tails describe the term $T(t)$ within 10% (resp. 1%) accuracy for times greater than about 15 (80), the term $T^2J(t)$ from $t=26$ (120) on and the other two from $t=40$ (175) on. For the 3D model these numbers are $t=20$ (57) for T, 25 (80) for T^2J, and 35 (100) for the terms cubic in T. The difference with the 2D case shows the slow logarithmic convergence in two dimensions.

These data (in fact, the dependence on the power of T) can be understood from the number of ring collisions (return visits to the same scatterer) involved in each of these terms. The powers of T account for the number of visits of the RW to a scatterer. In the term T there is only one scatterer involved, since it is the linear c term; for T^2J the RW visits first scatterer 1 and then scatterer 2 and subsequently moves away from the pair of scatterers. For the other two terms T^3J^2 and T^3I the RW returns to the first scatterer before hopping away. Only after each individual ring collision has reached its asymptotic form can the VACF assume its asymptotic

behavior. As the lattice sums involve more crossings between the two scatterers, we expect that the asymptotic regime for these contributions will be reached at a still later time.

Also for the lattice sum contributions we can calculate the dominant long-time behavior analytically. This is done by formally taking the derivative of the lattice sums in (2.16) with respect to J. The long-time tail is then expressed in that of J (J appears through T and $R = TG$, and the nonanalytic part of G_{xx} for small z is equal to $\delta G_{xx} = 2d\delta J$, and $\delta G_{xy} = 0$; see Ref. 13).

Subsequently, the expressions can be evaluated numerically along the same lines as the static diffusion coefficient (cf. Section 4 of this paper). For the percolation case $b = 1$ we find $\Sigma_{xx} = 0.21360t^{-2}$ and $\Sigma_{xy} = 0.06832t^{-2}$ for $d = 2$ and $\Sigma_{xx} = 0.01775t^{-5/2}$ and $\Sigma_{xy} = 0.002103t^{-5/2}$ for the 3D case, as these terms appear in (2.16), i.e., before taking out the factor of $1/2d$ [cf. Eq. (7.1)]. The deviation from these asymptotics is within 20% for times greater than $t = 215$ for both sums in two dimensions and is about 14% for $t = 300$. In 3D the sum Σ_{xx} has approached the asymptotic within 20% for $t = 160$, the Σ_{xy} lattice sum for $t = 250$. The $t = 300$ deviations are 13.6% and 17.6%, respectively. The difference between xx and xy reflects that Σ_{xx} is mainly determined by R^3 and Σ_{xy} by R^4 (we recall that $R \sim T$). This systematic difference is not observed for two dimensions; this might be explained by the strong influence of the subleading tail in that case.

For the lattice sums, the subleading long-time tails have not been calculated. This would be a very elaborate calculation because one needs to extract analytically the $O(z^2 \ln^2 z)$ and $O(z^2 \ln z)$ terms from the lattice sums and next evaluate them numerically. Because this analysis involves the $O(z)$ part of $G_{xx}(\mathbf{n}, z)$ [essentially the integral $\int_q \omega^{-2} \exp(-i\mathbf{nq})$] this numerical evaluation will be most easily performed using recursion formulas for this term that involve next nearest neighbor sites, where the static diffusion coefficient and the dominant tail of the lattice sums were calculated using nearest neighbor recursion relations (see Sections 3 and 4 and the Appendix). This indicates the amount of the work that has to be done.

The results for the diffusion coefficient can be compared with the results for the static diffusion coefficient (Section 4), because $D(\infty)$ should be equal to the static D. As we do not have results for t greater than 300, we compare the $t = 300$ values of Table III with the static values (Table II). The most difficult part to calculate is that coming from the lattice sums, which are the only contributions for the $O(c^2)$ term at $b = 1$. We looked in detail at the results for different values of b. Here, it suffices to discuss the percolation case. For three dimensions we clearly have approached the asymptotic regime within 1%. For two dimensions the difference can be

explained by the finiteness of $t = 300$. Considering the total lattice sum contribution, we fitted the form

$$\Sigma(t) = \Sigma(\infty) + 0.28192 t^{-1}[1 + Bt^{-1} \ln(t/\tau)]$$

to the data from $t \simeq 150$ to 300, yielding reasonable values of B and τ: 40 and 60, respectively.

As an illustration, we plot in Fig. 5 the total contribution to the time-dependent diffusion coefficient $D(t)$ in (7.1) at some finite values of the impurity concentration c. For the 2D bond model studied here computer simulations have been performed by Brey,[23] leading to results that agree, within the statistical errors, with our calculations. Note that D axis in Fig. 5 is linear; we have taken out the Enskog part and divided the remainder by c, resulting in $\bar{\alpha}_1(t) + \alpha_2(t)\, c$. The values for the concentration are taken equal to 0.01, 0.20, and 0.40. We recall that at $c = 0.40$ the density expansion is not expected to be valid in all detail.

To conclude, we note that for negative b values, corresponding to impurity bonds with a conductivity greater than that of the host lattice, it is also possible to calculate the first-order term (T). In that case, in addition to the branch cut from -2 to 0, we have to take into account a pole at z_0, given by

$$1 - bJ(z_0) = 0$$

From the structure of J, one easily concludes that this pole lies on the real axis left from -2. For $d = 2$, the pole is present for any $b < 0$, while for $d = 3$, b has to be less than -1.4758, as $J_3(z)$ (for $z < -2$) lies between -0.6776 and 0.

For the $O(c^2)$ terms we have not been able to obtain good results for negative b values. These are found to cause numerical instabilities. The results for $O(c)$ are reported in Ref. 13 for the 2D case. As the $O(c)$ results for three dimensions do not lead to essentially different features, we will not discuss them in this paper, which mainly considers second-order density effects.

Finally, we checked the accuracy of the numerical results by means of the relation (2.17), valid for the percolation case. As for all other b values, we calculated the terms T^2J, T^3J, and T^3J^2 separately and checked if their sum (using the appropriate weight factors) would give zero. The terms have been calculated independently. The result of the summation is a number that varies from 10^{-7} to 10^{-11} for small to large (near 300) values of the time. The separate terms have magnitudes of the order of 10^{-1} to 10^{-6}, thus having a rough five-digit accuracy over the whole time interval.

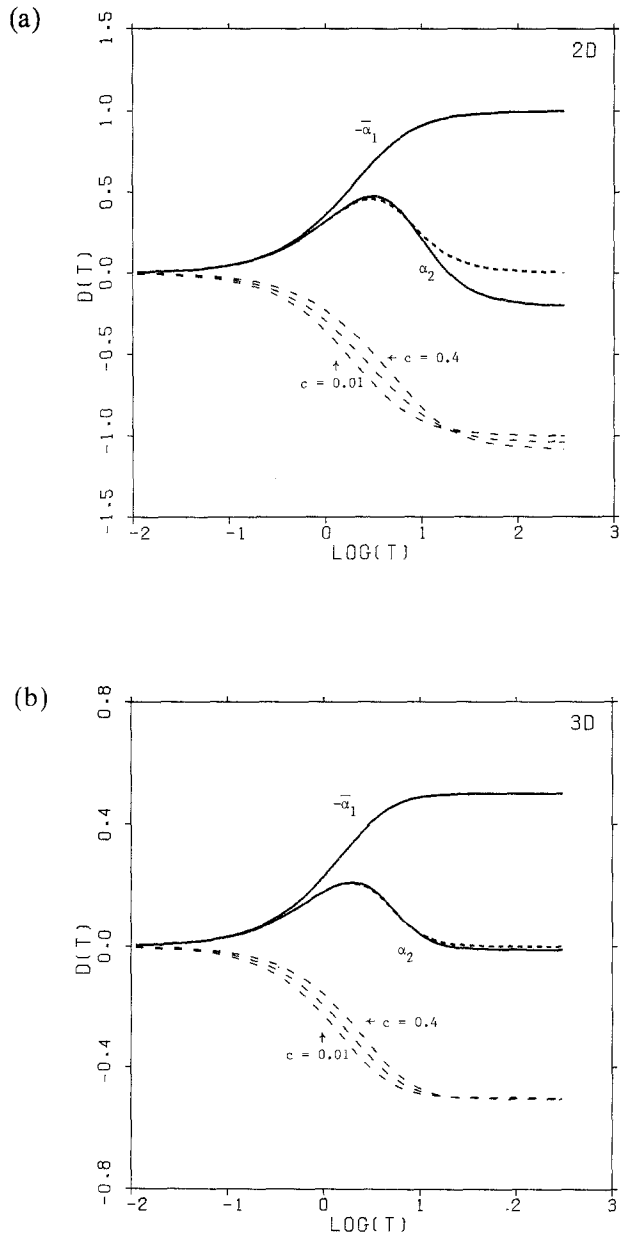

Fig. 5. Contributions to time-dependent diffusion coefficient $D(t)$ in Eq. (7.1). Upper part has the same legend as Fig. 3a.; lower part shows $\bar{\alpha}_1(t) + c\alpha_2(t)$ for $c = 0.01$, 0.20, and 0.40 (from left to right). (a) 2D, (b) 3D.

APPENDIX

In this Appendix we report the steps needed to calculate the $\hat{p}_d(\mathbf{n}, z)$ defined by (3.2) for the whole lattice of $\mathbf{n}$ vectors. In doing so, we rely heavily on Morita.[15]

First, $\hat{p}_2(0, 0, z)$ and $\hat{p}_2(1, 1, z)$ are given by

$$\hat{p}_2(0, 0, z) = \frac{2}{\pi(1+z)} K\left[\frac{1}{(1+z)^2}\right] \tag{A.1}$$

$$\hat{p}_2(1, 1, z) = \frac{2}{\pi(1+z)} \left\{ [2(1+z)^2 - 1] K\left[\frac{1}{(1+z)^2}\right] - 2(1+z)^2 E\left[\frac{1}{(1+z)^2}\right] \right\} \tag{A.2}$$

using the definitions of the complete elliptic integrals of the first (K) and second (E) kinds as defined by Abramowitz and Stegun.[21] From these expressions it is clear that for $z = -1$ we have a singularity, as K diverges logarithmically for argument near unity. In addition, the multiplicative factor in (A.1) differs in sign for z greater, resp. smaller, than -1, leading to a change from $-\infty$ to $+\infty$ for the real part; for the imaginary part this change in sign is canceled by complex conjugation of the argument as z goes through -1. Clearly, the same comments apply to the terms in (A.2) containing K. This kind of discontinuous behavior is shown by $\hat{p}_2$ for all lattice sites, as follows from the recurrence relations to be discussed in the following. Physically they can be seen as the analogue of the Van Hove singularities appearing in phonon spectra of harmonic crystals.[24] There the saddle points q_s in the parametrized surface $\omega(\mathbf{q})$ ($\mathbf{q} \in 1\text{BZ}$) [cf. Eq. (2.9)] give the location of the singularities in the spectrum: $\omega(\mathbf{q}_s) = 1$ for 2D; $\omega(\mathbf{q}_s) = 2/3$ or $4/3$ for 3D.

Next, the $\hat{p}_2(l, l, z)$ follow from [see Morita,[15] Eq. (3.8)]

$$\hat{p}_2(l+1, l+1, z) = \frac{4l}{2l+1} [2(1+z)^2 - 1] \hat{p}_2(l, l, z) - \frac{2l-1}{2l+1} \hat{p}_2(l-1, l-1, z)$$

Proceeding, we have, using (3.3a),

$$\hat{p}_2(1, 0, z) = (1+z) \hat{p}_2(0, 0, z) - 1$$

and

$$\hat{p}_2(l+1, l, z) = 2(1+z) \hat{p}_2(l, l, z) - \hat{p}_2(l, l-1, z)$$

which is used to calculate $\hat{p}_2(l, m, z)$ on the line $m = l-1$ from 0 to l. Next, we calculate $\hat{p}_2(l, m, z)$ on the line $(l, 1)-(l, l)$, using

$$\hat{p}_2(l+1, m, z) = 4(1+z)\,\hat{p}_2(l, m, z) - \hat{p}_2(l-1, m, z) - \hat{p}_2(l, m+1, z) - \hat{p}_2(l, m-1, z) \qquad \text{for} \quad 0 < m < l$$

Finally, on the axes

$$\hat{p}_2(l+1, 0, z) = 4(1+z)\,\hat{p}_2(l, 0, z) - \hat{p}_2(l-1, 0, z) - 2\hat{p}_2(l, 1, z)$$

The values of $\hat{p}_2$ in the other seven half-quadrants follow by symmetry.

From these data for $\hat{p}_2(l, m, z)$ it is possible to calculate the $\hat{p}_3(l, m, n, z)$ for the, say, $n = 0$ plane, using the expression (4.4) in the body of the paper. In essence this is an integration of the $\hat{p}_2(l, m, z)$ over a part of the real axis. A closer look at Eq. (4.4) shows that now the "Van Hove" singularities appear at $z = -4/3$ and $-2/3$, and are weaker, the latter because the logarithmic behavior of the two-dimensional lattice functions is integrated.

Once we have $\hat{p}_3(l, m, 0, z)$, the whole 3D lattice follows by

$$\hat{p}_3(l, m, 1, z) = 6(1+z)\,\hat{p}_3(l, m, 0, z) - 6\delta_{l0}\delta_{m0} - \hat{p}_3(l+1, m, 0, z) - \hat{p}_3(l-1, m, 0, z) - \hat{p}_3(l, m+1, 0, z) - \hat{p}_3(l, m-1, 0, z)$$

and, for $n \geqslant 1$,

$$\hat{p}_3(l, m, n+1, z) = 6(1+z)\,\hat{p}_3(l, m, n, z) - \hat{p}_3(l, m, n-1, z) - \hat{p}_3(l+1, m, n, z) - \hat{p}_3(l-1, m, n, z) - \hat{p}_3(l, m+1, n, z) - \hat{p}_3(l, m-1, n, z)$$

The $\hat{p}_3(\mathbf{n}, z)$ for the remaining regions of the lattice follow by symmetry.

The expressions (A.1) and (A.2) are valid for arbitrary complex value of z. However, for z or k^2 just below the branch cut it is more convenient to use the analytic continuations of the elliptic integrals, which imply the replacement of $K(1/k^2)$ and $E(1/k^2)$ by[15]

$$K(1/k^2) = k[K(k^2) + iK(1-k^2)]$$

$$E(1/k^2) = 1/k[E(k^2) - iE(1-k^2) - (1-k^2)\,K(k^2) + ik^2K(1-k^2)]$$

For the evaluation of the $\hat{p}_3(\mathbf{n}, z)$, we have to divide the integration in (3.4) into several intervals, where different expressions for the $\hat{p}_2(\mathbf{n}, z)$ have to be

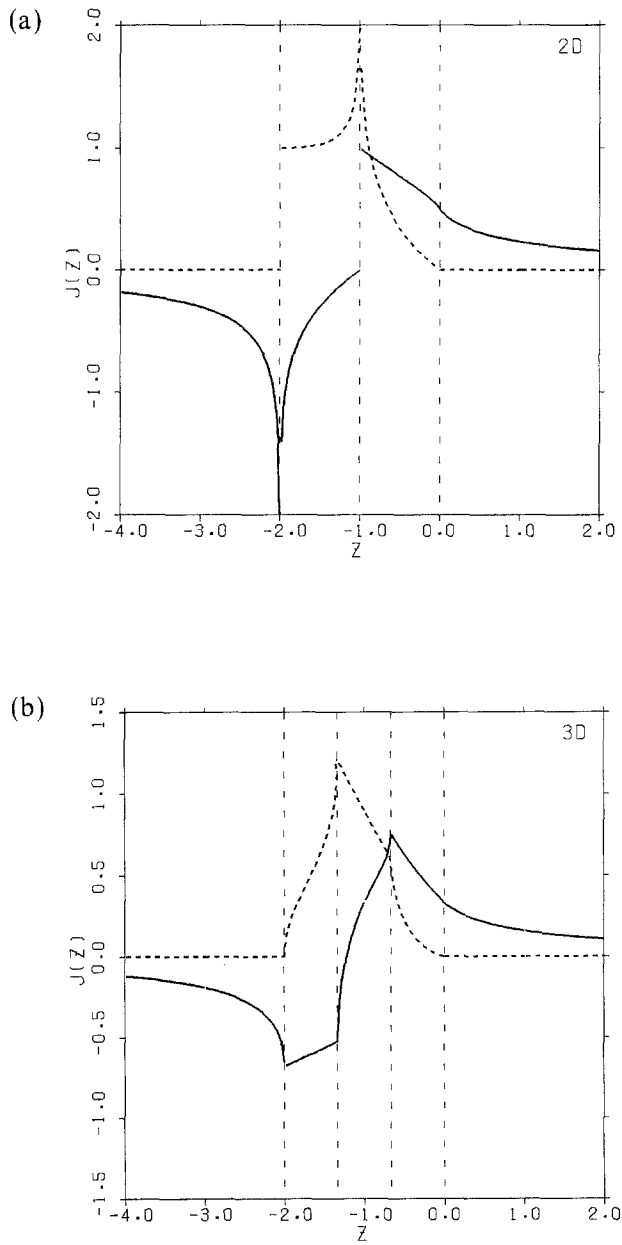

Fig. 6. Ring collision integral $J(z)$ for $z = s - i0$, $-4 < s < 2$. (—) Real part and (- -) imaginary part. Note the location of the "Van Hove" singularities at (a) -1 for 2D and (b) $-2/3$ and $-4/3$ for 3D.

used.[25] From the definition of the complete elliptic integrals it is clear that they obey the symmetry relations

$$K(k^{*2}) = K^*(k^2), \qquad K((-k_R + ik_I)^2) = K^*((k_R + ik_I)^2)$$

These lead to the symmetry relations for the real and imaginary parts of $\hat{p}(\mathbf{0}, z)$, for $d = 2, 3$,

$$\hat{p}_R(\mathbf{0}, -1 - s - i\varepsilon) = -\hat{p}_R(\mathbf{0}, -1 + s - i\varepsilon)$$
$$\hat{p}_I(\mathbf{0}, -1 - s - i\varepsilon) = \hat{p}_I(\mathbf{0}, -1 + s - i\varepsilon)$$

Using these relations in combination with the recursion formulas, we obtain insight into how to apply the subtraction technique to the calculation of $\hat{p}_3(\mathbf{n}, z)$ for arbitrary lattice site $\mathbf{n}$.

For illustration we investigate the structure of $J(z)$ in more detail. $J(z)$ follows from the previous results by writing

$$J(z) = \frac{1}{d}\int_{\mathbf{q}} \frac{\omega(\mathbf{q})}{z + \omega(\mathbf{q})} = \frac{1}{d} - \frac{z}{d}\int_{\mathbf{q}} \frac{1}{z + \omega(\mathbf{q})}$$
$$= \frac{1}{d}[1 - z\hat{p}(\mathbf{0}, z)]$$

The 2D and 3D cases are plotted in Figs. 6a and 6b, respectively, where the dashed lines represent the imaginary parts.

ACKNOWLEDGMENTS

The authors want to thank J. W. Dufty for stimulating discussions. The work of one of us (G. A. v. V.) is part of a research program of the Stichting voor Fundamenteel Onderzoek der Materie (FOM), which is financially supported by the Nederlandse Organisatie voor Zuiver-Wetenschappelijk Onderzoek (ZWO). The authors also thank the Physics Department of the University of Florida for its hospitality during the winter of 1986–1987, where part of this work was carried out. This research was supported in part by National Science Foundation grant CHE-8411932.

REFERENCES

1. E. H. Hauge, in *Transport Phenomena*, G. Kirczenov and J. Marro, eds. (Springer-Verlag, Berlin, 1974), p. 338; J. R. Dorfman and H. van Beijeren, in *Statistical Mechanics*, Part B. *Time Dependent Processes*, B. J. Berne, ed. (Plenum Press, New York, 1977); M. H. Ernst,

in *Recent Developments in Nonequilibrium Thermodynamics: Fluids and Related Topics*, J. Casas-Vasquez, D. Jou, and J. M. Rubi, eds. (Springer-Verlag, Berlin, 1986), p. 175.
2. Th. M. Nieuwenhuizen, P. F. J. van Velthoven, and M. H. Ernst, *Phys. Rev. Lett.* **57**:2477 (1986).
3. D. Frenkel, *Phys. Lett. A* **121**:385 (1987).
4. M. H. Ernst, P. F. J. van Velthoven, and Th. M. Nieuwenhuizen, *J. Phys. A* **20**:947 (1986).
5. M. H. Ernst and P. F. J. van Velthoven, *J. Stat. Phys.* **45**:1001 (1986).
6. V. K. S. Shante and S. Kirkpatrick, *Adv. Phys.* **20**:325 (1971); S. Kirkpatrick, *Rev. Mod. Phys.* **45**:574 (1973); in *Ill-Condensed Matter*, B. Balian, K. Maynard, and G. Toulouse, eds. (North-Holland, Amsterdam, 1979).
7. T. Odagaki, M. Lax, and A. Puri, *Phys. Rev. B* **28**:2755 (1983); T. Odagaki, *Phys. Rev. B* **33**:544 (1986).
8. M. Sahimi, B. D. Hughes, L. E. Scriven, and H. T. Davis, *J. Chem. Phys.* **78**:6849 (1983).
9. J. W. Haus and K. W. Kehr, *Phys. Rep.* (1987), to appear.
10. U. M. S. Costa, C. Tsallis, and G. Schwachheim, *Phys. Rev. B* **33**:510 (1986).
11. A. B. Harris and S. Kirkpatrick, *Phys. Rev. B* **16**:542 (1977).
12. J. B. T. M. Roerdink and K. E. Schuler, *J. Stat. Phys.* **41**:581 (1985); J. B. T. M. Roerdink, *Physica* **132A** (1985).
13. M. H. Ernst, *J. Stat. Phys.* **48**:645 (1987).
14. D. C. Hong, H. E. Stanley, A. Coniglio, and A. Bunde, *Phys. Rev. B* **33**:4564 (1986).
15. T. Morita, *J. Math. Phys.* **12**:1744 (1971).
16. G. L. Montet, *Phys. Rev. B* **7**:650 (1973).
17. G. N. Watson, *Q. J. Math.* **10**:266 (1939).
18. M. H. Ernst, *Physica* **140A**:390 (1986).
19. J. P. Straley, *Phys. Rev. B* **15**:5733 (1977).
20. K. Golden and G. Papanicolaou, *Commun. Math. Phys.* **90**:473–491 (1983).
21. M. Abramowitz and I. Stegun, *Handbook of Mathematical Functions* (Dover, New York, 1970).
22. M. H. Ernst, G. A. van Velzen, and J. W. Dufty, *Physica A*, 1987.
23. J. J. Brey, to be submitted.
24. N. W. Ashcroft and N. D. Mermin, *Solid State Physics* (Saunders College, Philadelphia, 1976).
25. T. Morita and T. Horiguchi, *J. Math. Phys.* **12**:981 (1971).